JOURNAL OF MATERIALS SCIENCE 27 (1992) 1883–1891

Structure and mechanical behaviour of short glass fibre-reinforced ethylene–tetrafluoroethylene copolymers

Part II *Description of the mechanical behaviour using rheological models*

E. M. WEIS, W. WILKE
Abteilung für Experimentelle Physik, Universität Ulm, Albert Einstein-Allee 11, D-7900 Ulm, Germany

The mechanical behaviour of a copolymer, consisting of ethylene, tetrafluoroethylene, hexafluoropropylene and perfluoropropylvinylether, unfilled and filled with short glass fibres has been investigated for strains less than 5%. Different deformation modes at room temperature and at 80 °C were recorded with a video system. The resulting stress–strain, relaxation and shrinkage curves are described with a model consisting of seven basic rheological elements of three different types: spring (Hooke model), dashpot (Newton model) and slip-element (St. Vénant model). This seven-element model gives a very good approximation of all the investigated deformation modes and allows an interpretation of relaxation and retardation times of polymer segments. The plastic deformation, described by the slip-element, is assumed to be caused by slip processes in the highly disordered crystallites of the copolymer matrix.

1. Introduction

Ethylene–tetrafluoroethylene copolymers (ETFE) show very remarkable mechanical, chemical and thermal properties. In Part I [1] we found, that when filled with short glass fibres, the mechanical properties of the studied quaterpolymer, which are good in the unfilled state, are further improved. This effect is due to the influence of the fibres on the superstructure of the matrix material, whilst the crystal structure, characterized by great longitudinal disorder, as well as the crystallinity are not changed. Because of the high degree of disorder in the crystallites, this polymer does not correspond to semicrystalline polymers in the usual sense, where we have a disordered amorphous phase and a highly ordered crystalline phase.

Our aim was to find a simple way of describing the mechanical behaviour for small strains, where fibre debonding has not yet occurred. The deformation region below the yield-point was of special interest. Large deformations and material failure were not considered. With the help of basical rheological elements we wanted to relate the obtained relaxation and retardation times to the microscopic characteristics of the material. In order to obtain as much information as possible, different kinds of deformation processes were carried out.

2. Experimental procedure

2.1. Samples

The chemical composition of the studied matrix material (as provided by Hoechst) was: 49.2 mol % ethylene (ET); 47.0 mol % tetrafluoroethylene (TFE); 3.6 mol % hexafluoropropylene (HFP); 0.17 mol % perfluoropropylvinylether (PPVE). The characteristic data of this material and of the glass fibres (diameter 10 μm, aspect ratio 1.20) used for filling, are given in [1].

The geometry of the investigated specimens, very important for this study to determine the strain values in the correct way, is shown in Fig. 1.

2.2. Deformation processes

For the unfilled material and filler contents, w_f, of 10 and 20 wt %, a set of experiments was conducted at testing temperatures of 23 and 80 °C (the method of

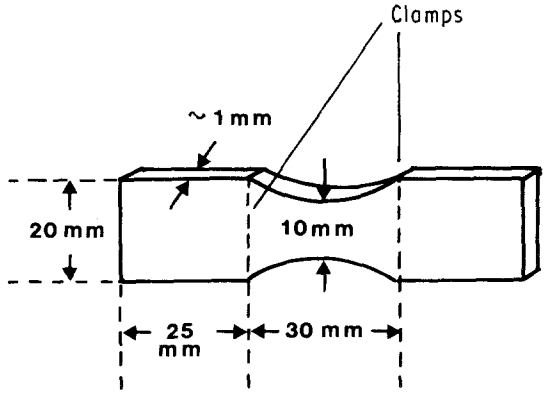

Figure 1 Geometry of the used specimen.

determinating stress, σ, and strain, e, will be described in the next section).

2.2.1. Uniaxial tensile test (Fig. 2)

First a uniaxial tensile test (deformation rate set at the testing machine $2.78 \times 10^{-4} s^{-1}$) was carried out until the yield-point (e_y, σ_y) was reached (I). From the resultant stress–strain curve, the value for the stress, σ_0, at a strain of about 4% was determined, in order to have a measure of the point at which to interrupt the following processes at about equivalent strains.

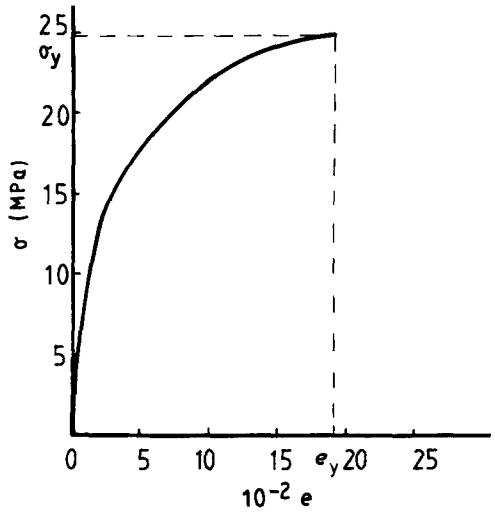

Figure 2 Uniaxial tensile test up to the yield point (Process I).

2.2.2. Relaxation test (Fig. 3)

A uniaxial tensile test (II) made under the same conditions as for the uniaxial tensile test, was stopped at σ_0 (Fig. 3a). The strain, e, was then held at a constant value, e_0, and the development of stress with increasing time, t, was recorded (III) for about 1 h (Fig. 3b).

2.2.3. Cycle with subsequent relaxation test (Fig. 4)

After stopping the tensile test at σ_0(IV) the specimen was relaxed in a controlled manner: the clamps were moved together with the same absolute value of the set velocity ($v = -2.78 \times 10^{-4} s^{-1}$) until the stress reached zero (V). The stress–strain curve was recorded (Fig. 4a). When zero stress was reached, the length of the sample (strain e_b) was held constant and the increasing stress, σ, with increasing time, t, was recorded for about $\frac{1}{2}$ h (VI, Fig. 4b).

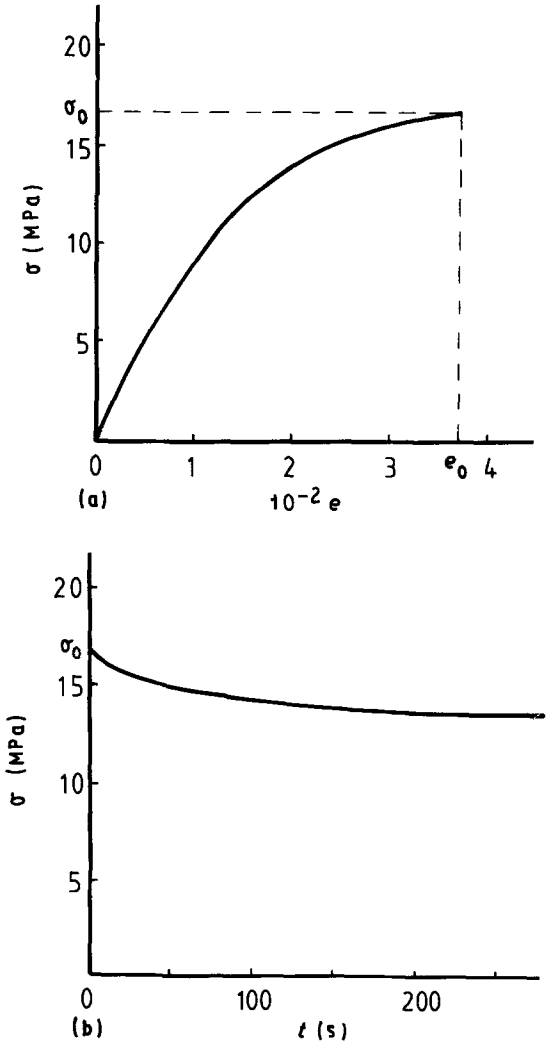

Figure 3 Relaxation experiment: (a) Process II, (b) Process III.

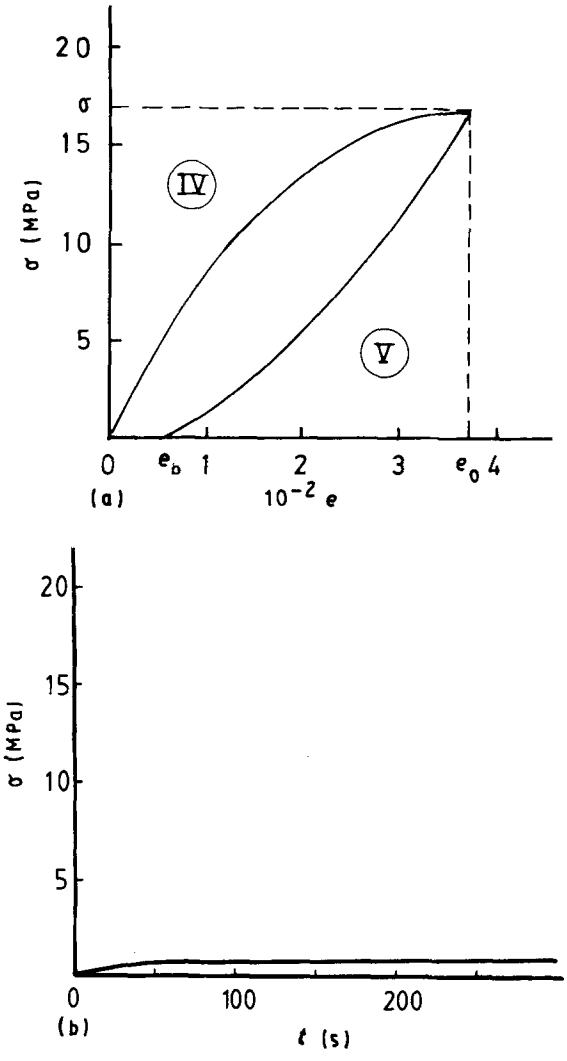

Figure 4 Cycle and relaxation experiment: (a) Processes IV and V, (b) Process VI.

2.2.4. Retardation test (Fig. 5)

After the tensile test was stopped at σ_0(VII) (Fig. 5a), one of the clamps, fixing the specimen, was opened, so that the sample was able to shrink freely (Fig. 5b). It was observed that when the clamp was opened, the sample immediately shrunk from e_0 to e_s. The strain, e, then diminished with increasing time, t (VIII).

In order to ensure that in the deformation region of interest no physical damage occurred, acoustic emission experiments were carried out during uniaxial tensile tests at room temperature. Only in the case of the sample filled with 20 wt % fibres was acoustic emission activity recorded towards the end of the examined deformation region. This fact must be kept in mind, when interpreting the results.

2.3. Measurement of strain

As opposed to the mechanical experiments described in Part I [1], where the relative behaviour of filled to unfilled material was of interest, it is necessary here to determine the true strain, in order to describe the mechanical behaviour. In Part I, the distance between the clamps, fixing the specimen, was used as a measure of strain, but this determines (see Fig. 1) only a mean value over the specimen. Thus for the computation the true strain, e, in the centre of the specimen, measured with the help of a video camera, was used. As shown in Fig. 6, the centre of the specimen was marked with lines, a distance, l, of about 1 mm apart (the exact value measured in pixel points on the screen in the unstretched state). Using a video camera, this part of the specimen was recorded during deformation and therefore it was possible to determine the strain e(t). The applied load, F, and the time, t, were also recorded. Thus from each video picture it was possible to compute the following data:

strain $e = (l - l_0)/l_0$; applied load, F; cross-section, A_0 (unstretched specimen).

The slope of $\sigma(e)$ at the origin gives modulus E.

As expected very different values were obtained (see Fig. 7) when comparing the stress–strain curves of ETFE using the clamp distance and the video-records for the evaluation of the strain.

For the computation not only the true strain, e, but also the development of e with time, t, is required. To obtain this dependence, $e(t)$, in analytical form the

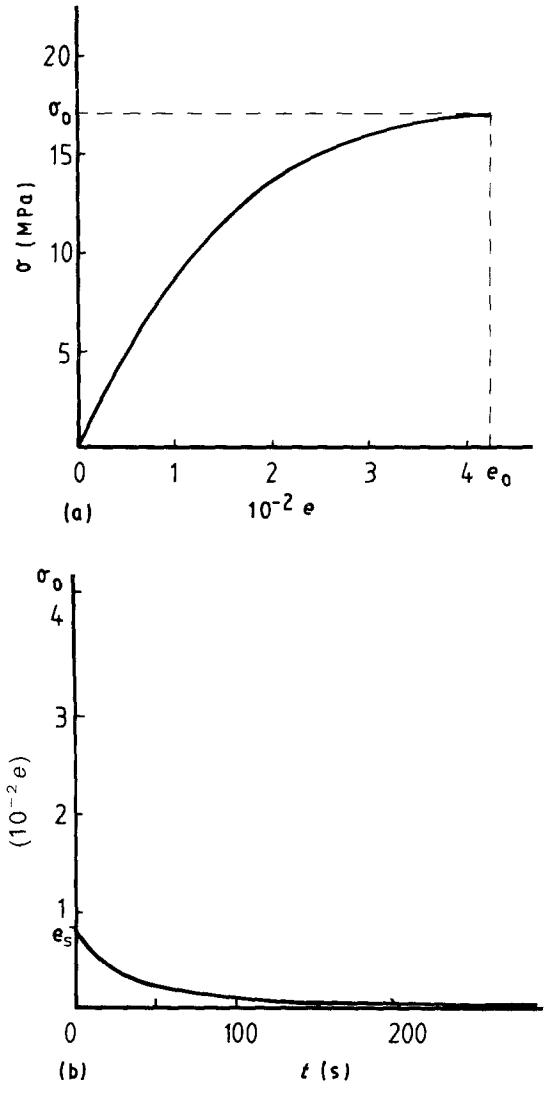

Figure 5 Retardation experiment: (a) Process VII, (b) Process VIII.

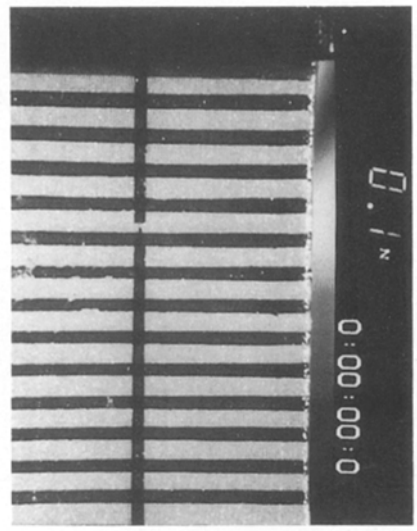

Figure 6 Video picture of the specimen during deformation with faded-in applied load, F (upper left corner) and time, t (upper right corner).

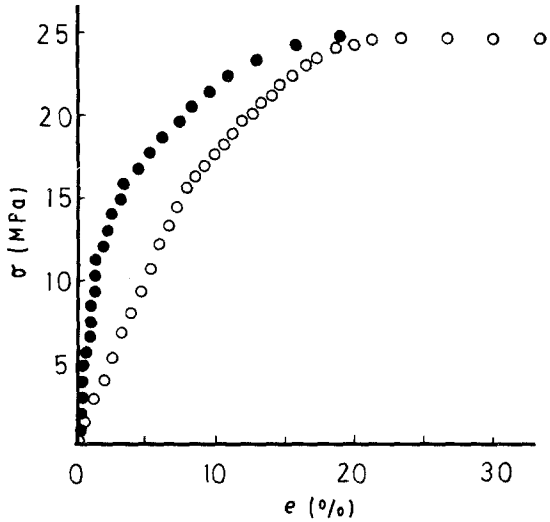

Figure 7 Comparison of stress–strain curves of the same measurement ($v_f = 0$, $T = 23\,^{\circ}C$), evaluated (●) using video records and (○) using distance between clamps.

following approach was used

$$e = bt^2 + vt \quad (1)$$

which reproduces the experimental data very well, as can be seen in Fig. 8.

When evaluating the data for the return phase in the cycle, it was found that the dependence $e(t)$ was nearly linear

$$e = -|v_R|t \quad (2)$$

The values of v_R, lying in the same order as the set value at the testing machine, and the values for b are given in Table I (in the experiments, v always equals zero).

3. The applied model

The model used to describe the deformation processes discussed above, consists of seven basic elements of three different types (see Fig. 9). Before discussing the applied model, these three basic elements, which are shown in Fig. 10, are examined. The dependences, $\sigma(e)$, for these elements are given as follows [2, 3]

(a) spring (Hooke model): $\sigma = Ee$ (3)

(b) dash-pot (Newton model): $\sigma = \eta\dot{e}$ (4)

(c) slip-element (St. Venant model):

$$|\sigma| \leq \sigma_p \quad \dot{e} = 0$$

$$\sigma = \sigma_p \operatorname{sign}(\dot{e}) \quad \dot{e} \neq 0 \quad (5)$$

For a given arrangement of two elements, characterized by (σ_1, e_1) and (σ_2, e_2) a relation can be determined between the total stress, σ, and the total strain, e, by using the rules for addition:
for parallel arrangement, $e = e_1 = e_2$, $\sigma = \sigma_1 + \sigma_2$ and for serial arrangement, $e = e_1 + e_2$, $\sigma = \sigma_1 = \sigma_2$.

Thus it is possible to compute any given arrangement of several elements. For the model presented in Fig. 9, the relation between σ and e is given by a linear differential equation of the second order, which is valid in the case where the slip-element remains at a

TABLE I Strain rates, determined using Equations 1 and 2

w_f(%)	T(°C)	$b(10^{-7}\,s^{-2})$	$v_R(10^{-4}\,s^{-1})$
0	23	1.93	2.52
10	23	1.57	2.12
20	23	1.31	1.92
0	80	2.66	2.68
10	80	2.54	2.30
20	80	1.56	2.93

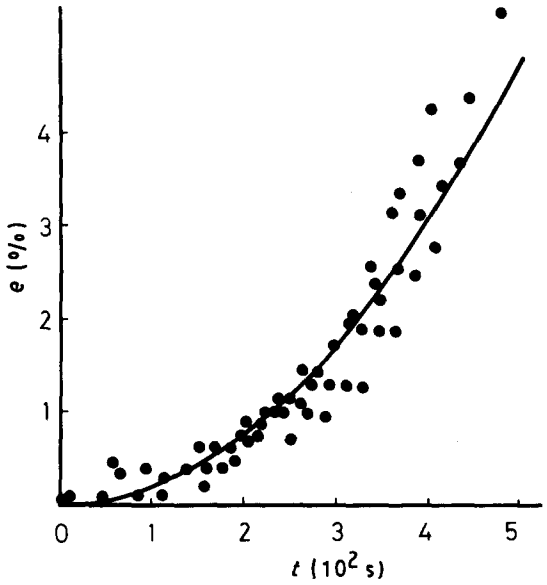

Figure 8 Time-dependent development of strain in the middle of the specimen ($v_f = 0$, $T = 23\,°C$): (●) experimental data (video-evaluated) (—) fitted, using Equation 1.

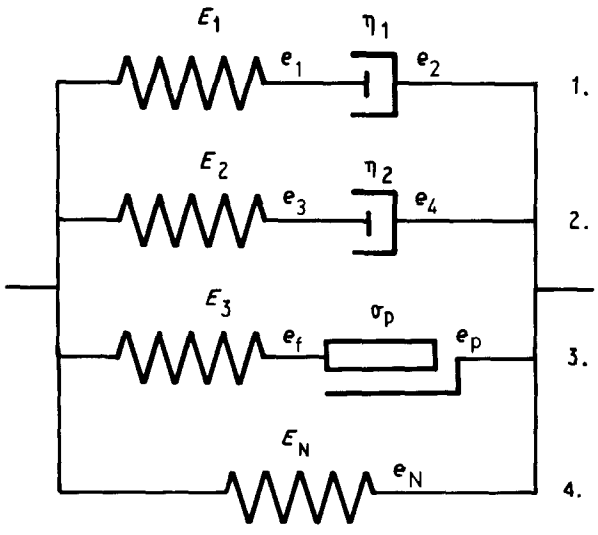

Figure 9 Seven-element model.

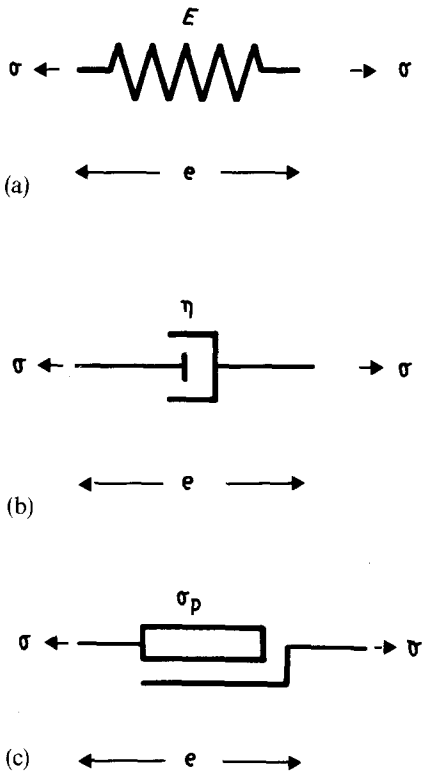

Figure 10 Basic elements of rheology. (a) Spring, (b) Dash-pot, (c) Slip element.

given position, e_{p0}

$$\ddot{\sigma} + \dot{\sigma}\left(\frac{1}{\tau_1} + \frac{1}{\tau_2}\right) + \sigma\left(\frac{1}{\tau_1\tau_2}\right) = \ddot{e}E_{ges} + \dot{e}\left(\frac{E_{ges} - E_1}{\tau_1} + \frac{E_{ges} - E_2}{\tau_2}\right) + e\frac{E_3 + E_N}{\tau_1\tau_2} - e_{p0}\frac{E_3}{\tau_1\tau_2} \quad (6)$$

where

$$\tau_1 = \eta_1/E_1 \quad (7)$$

$$\tau_2 = \eta_2/E_2 \quad (8)$$

$$E_{ges} = E_1 + E_2 + E_3 + E_N \quad (9)$$

Before considering the above specified deformation processes in detail, the physical meaning of this model should be examined. The model used consists of seven elements, arranged in four branches, numbered 1–4 (Fig. 9.) In this model only the individual branches as a whole have a physical meaning and not just single elements.

From thermodynamical considerations [4] it is known that Branches 1 and 2, so called Maxwell elements, in combination with Branch 4 describe internal relaxation processes, which can be related to microscopic characteristics using, for example, a very simplified model described by Malmeisters *et al.* [5]. There, stress-induced changes in the position of polymer segments are responsible for the relaxation processes. Maxwell elements, having different relaxation times, τ, describe segments of different length. Attempts made to describe the experimental data with only one relaxation process failed, so the minimum number of Maxwell elements must be two. The combination of the slip element and the spring in the third branch offers the possibility to describe a slip process which does not begin before a given stress is reached. The present investigations enabled the observed slip process to be related to the crystals. Because the slip element describes an irreversible plastic deformation, this element does not move when the specimen is able to shrink (Processes V and VIII). The fourth branch, consisting of a single spring describes the elastic properties of the material and therefore characterizes the physical network.

Because the model used by Malmeisters describes the changes of segment-positions as a consequence of the applied stress, it cannot be assumed that the relaxation processes will remain the same when changing the direction of applied load, and especially that they will have the same relaxation times, τ. Furthermore, due to the plastic deformation, the reference state is changed. So in the present investigations the set of parameters is allowed to change when changing the tensile conditions, denoting the characteristic parameters as E_1, η_1, etc., of the first set (Processes I, II, III, IV, VII) without primes and of the second set (Processes V, VI, VIII) with a prime (E_1', η_1', etc.). Thus the simplest model which describes the present experimental data as well as required, is the seven-element model shown in Fig. 9 which has the possibility to change the set of parameters when changing the direction of the applied load.

The different deformation processes are now described.

3.1. Uniaxial tensile test (Figs 2, 3a, 4a, 5a)

Using the above characteristics for the development of strain e with time t, the following process conditions must be considered

$$e(t) = bt^2 + vt \quad (10)$$

In this case the easiest way to compute the σ–e relation is to solve the differential equations for the four branches of the seven-element model separately and then to sum the four contributions.

In this way the following result is obtained, where attention must be paid to the fact that below the critical strain, $e_g = \sigma_p/E_3$, the slip element remains at rest and for $e > e_g$ it moves

$$\sigma(e) = \sigma_1(e) + \sigma_2(e) + \sigma_3(e) + \sigma_4(e) \quad (11)$$

with

$$\sigma_1(e) = (2\eta_1\tau_1 b - \eta_1 v)(e^{-t/\tau_1} - 1) + 2\eta_1 bt$$

$$\sigma_2(e) = (2\eta_2\tau_2 b - \eta_2 v)(e^{-t/\tau_2} - 1) + 2\eta_2 bt$$

$$\sigma_3(e) = E_3 e \quad \text{for} \quad e \leq e_g$$

$$= \sigma_p = E_3 e_g \quad \text{for} \quad e > e_g$$

$$\sigma_4(e) = E_N e$$

$$t = \frac{1}{2b}[(v^2 + 4be)^{\frac{1}{2}} - v]$$

At the end of the uniaxial deformation we have time, t_0, and strain, e_0, and therefore also the total stress, $\sigma_0 = \sigma(e_0)$, and stresses for the individual branches $\sigma_{i0} = \sigma_i(e_0)$. If the strain e_0 reached is greater than e_g the new position of the slip element can be computed by

$$e_{p0} = e_0 - e_g \quad (12)$$

3.2. Stress relaxation, following the tensile test (Fig. 3b)

With the given condition for this process

$$e(t) = e_0 \quad (13)$$

the stress–strain relation is determined in the same way as before, adding up the contributions of the individual branches, giving

$$\sigma(t) = \sigma_1(t) + \sigma_2(t) + \sigma_3(t) + \sigma_4(t) \quad (14)$$

with

$$\sigma_1(t) = \sigma_{10} e^{-t/\tau_1}$$

$$\sigma_2(t) = \sigma_{20} e^{-t/\tau_2}$$

$$\sigma_3(t) = E_3 e_0 \quad \text{for} \quad e_0 \leq e_g$$

$$= \sigma_p = E_3 e_g \quad \text{for} \quad e_0 > e_g$$

$$\sigma_4(t) = E_N e_0$$

where e_0, σ_{10}, σ_{20} are given by the previous uniaxial tensile test.

3.3. Return phase of the cycle (Fig. 4a)

Here the second set of parameters, marked with a prime, is used. Using the process condition

$$e(t) = e_0 - |v_R|t \tag{15}$$

to solve the differential Equation 6 the following stress–strain relation is obtained:

$$\sigma(e) = \sigma_1(e) + \sigma_2(e) + \sigma_3(e) + \sigma_4(e) \tag{16}$$

with

$$\sigma_1(e) = (\sigma'_{10} + |v_R|\eta'_1)e^{-[1/\tau'_1|v_R|](e_0 - e)} - |v_R|\eta'_1$$

$$\sigma_2(e) = (\sigma'_{20} + |v_R|\eta'_2)e^{-[1/\tau'_2|v_R|](e_0 - e)} - |v_R|\eta'_2$$

$$\sigma_3(e) = E'_3(e - e_{p0})$$

$$\sigma_4(e) = E'_N e$$

Three facts should be noted here.

1. The slip element should not move during the return phase, i.e. it remains at its given positon e'_{p0}.

2. The contributions for the four branches cannot be simply added up, because the set of parameters changes. Therefore only the sum $\sigma_{10} + \sigma_{20}$ is given which results in one more free parameter when fitting the experimental data.

3. For solving the second-order differential equation two initial conditions are required. The first, $\sigma(e_0)$, is given by the condition that the total stress at the end of the tensile test should be the total stress at the beginning of return phase, and the second, describing the behaviour of σ at e_0, is chosen to be analogous to that for a five-element model where the third branch of the present seven-element model is absent.

3.4. Stress relaxation following the cycle (Fig. 4b)

From the relation for the return phase (Equation 16) the strain, e_b, can be determined, where the total stress reaches zero. So for the subsequent stress-relaxation the following condition applies:

$$e(t) = e_b \tag{17}$$

Because the set of parameters does not change, the contributions of the branches can again be summed and the σ–t relation can be obtained

$$\sigma(t) = \sigma_1(t) + \sigma_2(t) + \sigma_3(t) + \sigma_4(t) \tag{18}$$

with

$$\sigma_1(t) = \sigma^*_{10}e^{-t/\tau'_1}$$

$$\sigma_2(t) = \sigma^*_{20}e^{-t/\tau'_2}$$

$$\sigma_3(t) = E'_3(e_b - e_{p0})$$

$$\sigma_4(t) = E'_N e_b$$

with the constants σ^*_{i0} given as follows:

$$\sigma^*_{i0} = \sigma_i(e_b) = (\sigma'_{i0} + |v_R|\eta'_i)e^{-[1/\tau'_i|v_R|](e_0 - e_b)} - |v_R|\eta'_i$$

3.5. Retardation experiment

Using the second set of parameters and the condition

$$\sigma(t) = 0 \tag{18}$$

for the retardation experiment, a differential equation of second order in strain, e, is obtained. To solve this equation, two initial conditions are used. First

$$e(0) = e_s \tag{19}$$

where e_s is the strain given after the immediate shrinkage, and second the behaviour of e at $t = 0$. Here two factors are decisive: the longer one of the retardation times, τ_{2s}, and the difference in strain at the beginning ($e(0) = e_s$) and at the end ($e_\infty = e_{p0}E'_3/(E'_3 + E'_N)$) of the retardation process. So we assume

$$\dot{e}(0) = -\frac{1}{\tau'_{2s}}(e_s - e_\infty) \tag{20}$$

where $1/\tau'_{2s}$ is given as follows (determined by using $e(t) = \exp(-1/\tau'_{2s})$ to solve the homogeneous differential equation)

$$\frac{1}{\tau'_{2s}} = \left\{\frac{E'_{ges} - E'_1}{\tau'_1} + \frac{E'_{ges} - E'_2}{\tau'_2} - \left[\left(\frac{E'_{ges} - E'_1}{\tau'_1} + \frac{E'_{ges} - E'_2}{\tau'_2}\right)^2 - 4E'_{ges}\frac{E'_3 + E'_N}{\tau'_1\tau'_2}\right]^{1/2}\right\} \Big/ 2E'_{ges} \tag{21}$$

Using the above two conditions, for the development of strain, e, with time, t, we obtain

$$e(t) = \left(e_s - e_{p0}\frac{E'_3}{E'_3 + E'_N}\right)e^{-t/\tau'_{2s}} + e_{p0}\frac{E'_3}{E'_3 + E'_N} \tag{22}$$

Here it must be noted that because of the change in the set of parameters, the strain e_s is not determined and therefore we have one more free parameter when fitting the experimental data.

4. Comparison with experimental data and results

Regarding the deformation processes we recognize that there are eight partial processes (I–VIII) of five different kinds. To fit these parts all at once, a programme was developed that minimizes the following sum:

$$\sum_{i=I}^{VIII}\frac{g_i}{n_i}\sum_{j=1}^{n_i}[y_{ij}(x_{ij}) - y(x_{ij})]^2 \tag{23}$$

by varying the parameters, where n_i is the number of experimental data pairs (x_{ij}, y_{ij}) for process i; g_i is the weight factor of the process i, $y(x_{ij})$ is the theoretical values of y at the experimental points x_{ij}, computed for the different processes i using the above equations assigned as follows:

i =	I, II, IV, VII	Equation 11
i =	III	Equation 14
i =	V	Equation 16
i =	VI	Equation 18
i =	VIII	Equation 22

For more details see [6]; separate documentation of the programme is available from the authors.

As an example of the quality of the fits in Figs 11, 12

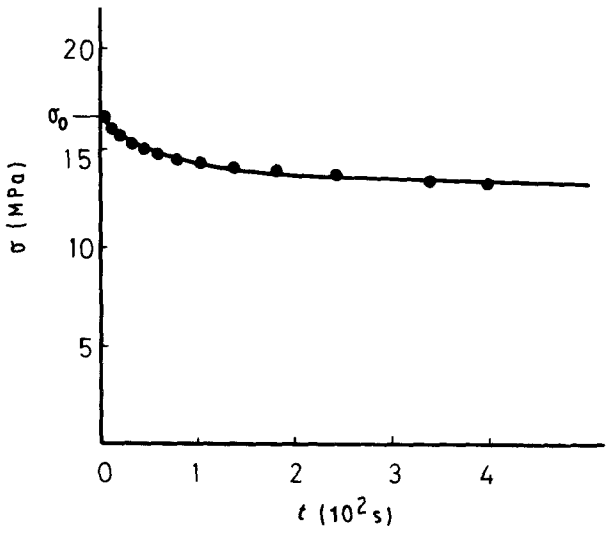

Figure 11 Fitted experimental data for $v_f = 0$, $T = 23\,^{\circ}C$, relaxation experiment (cf. Fig. 3).

and 13, theoretical curves compared with experimental data are shown for the measurement of an unfilled sample at 23 °C. For this fit and all the other fitted measurements the parameters giving best agreement with the experiment are listed in Table II. The errors are estimated to be smaller than 10%. In Table II the characteristic quantities of the dash-pots η are not listed because of greater physical importance of the combined quantities τ given by Equations 7 and 8. For the same reason the value of e_g is used to characterize the slip element.

5. Discussion

As can be seen from Table II, the modulus, E_{ges}, increases with increasing fibre content, w_f, indicating bonding between fibres and matrix. For the investigated composites, the critical fibre length, l_c, is smaller than the actual length, l. An estimation of l_c gives

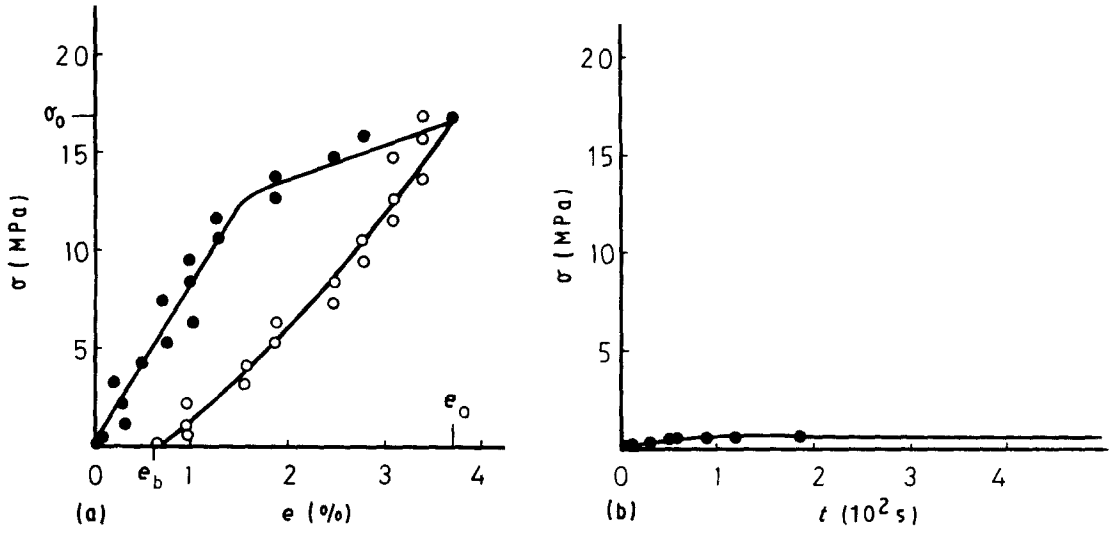

Figure 12 Fitted experimental data for $v_f = 0$, $T = 23\,^{\circ}C$ cycle plus relaxation experiment (cf. Fig. 4).

TABLE II Values obtained for the parameters of the seven-element model by fitting experimental data

	w_f at $T_v = 23\,^{\circ}C$			w_f at $T_v = 80\,^{\circ}C$		
	0 wt %	10 wt %	20 wt %	0 wt %	10 wt %	20 wt %
E_1(MPa)	71	132	155	55	68	80
τ_1 (s)	928	405	513	542	767	1090
E_2(MPa)	319	838	916	300	284	261
τ_2(s)	49	19	26	24	40	63
E_3(MPa)	580	697	1064	219	317	441
e_g(%)	1.55	1.38	1.07	2.11	1.37	1.57
E_N(MPa)	80	134	276	20	75	42
E'_1(MPa)	60	70	256	88	107	292
τ'_1(s)	201	141	58	550	265	777
E'_2(MPa)	327	473	375	153	281	192
τ'_2(s)	46	18	5	18	23	5
E'_3(MPa)	0	0	0	18	2	10
E'_N(MPa)	87	99	102	61	58	84
σ'_{10}(MPa)	0	0	0	1.1	0	4,8
e_s(%)	0.47	0.27	0.85	1.74	0.56	0.88
σ_p(MPa)	9.0	9.6	11.4	4.6	4.3	6.9
E_{ges}(MPa)	1050	1800	2311	594	744	825
E'_{ges}(MPa)	475	642	732	320	448	578

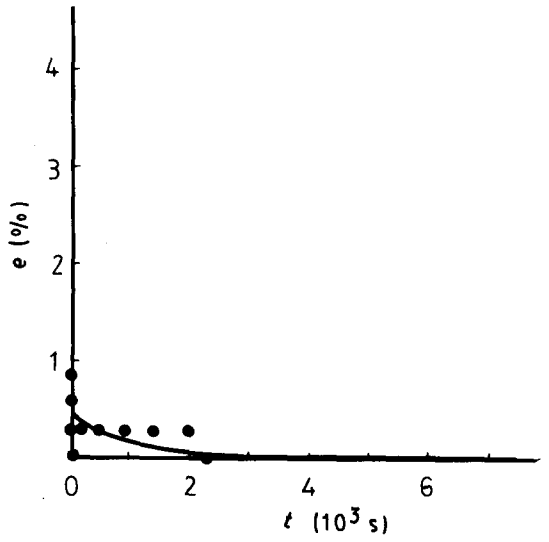

Figure 13 Fitted experimental data for $v_f = 0$, $T = 23\,^{\circ}C$ retardation experiment (cf. Fig. 5).

$l_c \sim 35\ \mu m$ and for l a mean value of $l \sim 100\ \mu m$ was found. The fibre modulus is $E_f = 77$ GPa. For the composite modulus, E_c, the following relation holds [7]:

$$E_c \approx \frac{1}{f} v_f E_f \left(1 - \frac{l_c}{2l}\right) + (1 - v_f) \underset{(l_c < l)}{E_m} \quad (24)$$

where E_m is the matrix modulus, v_f the volume content of the filler

$$\frac{1}{v_f} = 1 + \frac{\rho_f}{\rho_m}\left(\frac{1}{w_f} - 1\right) \quad (25)$$

where $\rho_{f,m}$ is the density of fibre, matrix, $f = 6$ for fibres with isotropic orientation, $f = 3$ for planar randomly oriented fibres.

Calculated f-values from the experimental data for $T_v = 20\,^{\circ}C$ are near $f = 6$, but for $T_v = 80\,^{\circ}C$ are much higher. This result means that for $T = 20\,^{\circ}C$ the adhesion between filler and matrix is strong and at $T = 80\,^{\circ}C$, weak. At $T = 80\,^{\circ}C$ the glass transition region of the ETFE matrix begins and therefore, as a result of the higher chain mobility, smaller stresses suffice to destroy the adhesion. The kind of bonding between fibre and matrix is very probably caused by the contraction during cooling. The samples show the effect of transcrystallinity [1], which is important for the composite behaviour [8]. By virtue of the transcrystallinity close contacts between the microscopically rough fibre surface and the polymer chains are possible. The discontinuity in the E-modulus between fibre and semicrystalline matrix is smeared out and therefore stress concentrations are lowered.

It is interesting to note, that all the above mechanical processes can be described with the relatively simple seven-element model. The viscoelastic part is characterized by two relaxation times, τ_i. This is an idealized picture; in reality we will have a spectrum of relaxation times. However, this simple model has the advantage that different processes can be described with analytical formulae and one can derive some material parameters from experiment. Because measurements were made with a definite strain rate, these relaxation times are typical for chain segment motions on this time scale. Creep experiments would give information about longer time scales. The viscoelastic deformation should be related to the amorphous part of the polymer matrix. The relatively long relaxation times indicate that the temperature during deformation lies below the glass transition temperature, T_g. Near T_g, at $T_v = 80\,^{\circ}C$, the relaxation times τ_1 and τ_2 increase with filler content, w_f. At this temperature the filler probably acts only as a geometrical hindrance for longer chain sequence mobility, whereas at $T = 23\,^{\circ}C$ the stronger adhesion and transcrystallinity masks this effect. Assuming a transient state model for the viscoelastic deformation [5], one would expect, that the relaxation times, τ_i', for the return phase are longer than the relaxation times τ_i. The experiments (Table II) show the opposite. However, $\tau_i' > \tau_i$ is only true, if the structure is not changed during the deformation. But in the present case we have a plastic deformation, described by the slip element. The onset of the plastic deformation is given by the strain e_g, in the range $e_g \sim 1$–2%. A non-negligible part of the irreversible deformation in the cycle (Fig. 12) is plastic deformation. The strain, σ_p, clearly is only a phenomenological mean value. On a microscopic scale there are large local fluctuations in the strains. The increase of σ_p at $w_f = 20\%$ can be explained on this basis. At this higher filler concentration, a local failure mechanism occur, which reduces local strain and the change in slope in the σ–e plot is shifted to a higher σ_p value.

The plastic deformation is associated with the crystalline part of the matrix. The crystals are longitudinally disordered, as shown by X-ray measurements [1]. That the melt enthalpies of the ETFE crystals are smaller than the melt enthalpies for PE and PTFE crystals also is an indication of this. Therefore, slip processes are easily initiated. Assuming that plastic deformation is a dislocation process [9], the dislocation density can be estimated from the irreversible dissipated energy in the plastic part of the deformation cycle. The calculated dislocation densities [10] are as expected. The pure elastic part of the deformation is described by E_N in the model. It is the "network" fraction of the deformation. The "network" is build, for example, by entanglements and crystals and fibres as netpoints. It was always found, that the pure elastic part $E_N(E_N')$ is smaller than $E_{ges}(E_{ges}')$. E_N increases with w_f (except for $T_v = 80\,^{\circ}C$, $w_f = 20\%$, where some failure may occur), showing that the fibres act like netpoints. The relative importance of the elastic deformation is higher for the return phase, for both temperatures $T_v = 23\,^{\circ}C$ and $T_v = 80\,^{\circ}C$. For $T_v = 23\,^{\circ}C$, from Table II, $E_{ges}/E_N \sim 13$, $E_{ges}'/E_N' \sim (5.5$–$7.2)$, and for $T_v = 80\,^{\circ}C$, $E_{ges}/E_N \sim (10$–$30)$, $E_{ges}'/E_N' \sim (5.2$–$7.7)$. This behaviour reflects the fact that the plastic deformation does not play any role in the return phase.

Acknowledgements

We are grateful for the support of the Bundesministerium für Forschung und Technologie, the Deutsche

Forschungsgemeinschaft and Hoechst AG and we thank Dr J. Marosfalvi, TU Budapest, for making the acoustic emission experiments.

References

1. E.-M. WEISS and W. WILKE, *J. Maters. Sci.* **27** (1992), in press.
2. I. M. WARD, "Mechanical Properties of Solid Polymers" (Wiley, Chichester, 1983).
3. A. KRAWIETZ, "Materialtheorie" (Springer, Berlin, 1986).
4. H. BAUR, "Einführung in die Thermodynamik der irreversiblen Prozesse" (Wissenschaftliche Buchgesellschaft, Darmstadt, 1984).
5. A. MALMEISTERS, V. TAMUZS and G. TETERS, "Mechanik der Polymerwerkstoffe" (Akademie, Berlin, 1977).
6. E.-M. WEIS, Doctoral Thesis (Dissertation), Universität Ulm (1988).
7. A. A. BERLIN, S. A. VOLFSON, N. S. ENIKOLOPIAN and S. S. NEGMATOV, "Principles of Polymer Composites" (Springer, Berlin 1986).
8. T. HE, R. PORTER, *J. Appl. Polym. Sci.* **35** (1988) 1945.
9. E.-M. RECK, H. SCHENK, W. WILKE, *Progr. Colloid Polym. Sci.* **71** (1985) 154.
10. A. PAYER, Thesis (Diploma), Universität Ulm (1990).

Received 3 December 1990
and accepted 13 May 1991